JOURNAL OF GEOPHYSICAL RESEARCH, VOL. 96, NO. B13, PAGES 21,887–21,892, DECEMBER 10, 1991

Sources of Unsteady Column Dynamics in Pyroclastic Flow Eruptions

GREG A. VALENTINE AND KENNETH H. WOHLETZ

Earth and Environmental Sciences Division, Los Alamos National Laboratory, Los Alamos, New Mexico

SUSAN W. KIEFFER

Department of Geology, Arizona State University, Tempe

During the first several minutes of an explosive volcanic eruption, the flow in the column above the vent is unsteady even if the discharge from the vent is steady. At a fixed location in the column, parameters such as temperature and ash content change with time until steady flow conditions are established. For conditions believed to be typical of fountain-forming silicic eruptions of intermediate volume, numerical simulations show unsteadiness in temperature, plume diameter, mass flux, vertical velocity, and particle concentration. In addition to the steady mass flux from the vent, we have identified three sources of mass and heat flux into the column: (1) recirculation of pyroclastic flow material into the base of the column (low elevation inward flow); (2) ash entrained from the top of the pyroclastic flow by atmospheric inflow back toward the column (higher-elevation inward flow); and (3) waves reflected within the pyroclastic flow if it encounters topographic obstacles. The thermal and mass flux pulses cause variations in column diameter and fountain height. Changing column diameter would be expected to be manifested in changes in fallout deposits (e.g., by shifts in clast isopleths). These temporal variations (if observed, for example, by satellite measurements of temperature pulses or pulses or inferred from field observations of deposit stratigraphy) could be misinterpreted as indicating source variations such as source mass flux, volatile content, or vent diameter, when, in fact, they result from fluid mechanical processes.

INTRODUCTION

In most theoretical models of volcanic eruption dynamics, constant discharge at the vent is assumed, and conditions during steady flow are examined (see review by *Woods* [1988]). These models can be used in a number of ways to infer eruption parameters. Examples include determination of column height from observations of deposit volume and eruption duration, calculation of mass fluxes from measured column heights, and relating variations in deposit stratigraphy to changing vent conditions during the eruption. Evidence of variations in column conditions or in the deposit stratigraphy has been attributed to mass flux variations at the vent caused by changes in magma volatile content and vent diameter [e.g., *Carey and Sparks*, 1986; *Woods*, 1988]. Application of steady state fluid dynamics theory to varying eruption parameters is valid when the change in vent parameters is much slower than the equilibration time of the column as a whole.

In this paper we examine temporal variations in column conditions that can occur even when vent mass flux is constant. These variations arise from phenomena that occur in the initial few minutes of an eruption as the column is developing over the vent and from later changes in column conditions as recirculation of material from pyroclastic flows occurs (Note that in this paper we use the term pyroclastic flow for any pyroclastic density current that flows laterally along the ground). We show that column temperature, diameter, and ash content vary as the column and pyroclastic flows develop, and we discuss how these variations may influence interpretation of remote observations of volcanic plumes and interpretation of deposits from eruptions.

Copyright 1991 by the American Geophysical Union.

Paper number 91JB02151.
0148-0227/91/91JB-02151$05.00

THEORETICAL APPROACH

In this numerical analysis the mass, momentum, and internal energy conservation equations for a compressible gas with dispersed particles are solved to simulate the large-scale dynamics of explosive eruptions. The conservation equations are solved separately for both the gas and the particles, which interact with each other via drag forces and heat transfer. The gas properties are represented by an ideal gas equation of state, and the particles are assumed to be incompressible. Turbulence is modeled by a simple eddy viscosity formulation. Specific material properties, equations of state, and description of the governing partial differential equations are given by *Valentine and Wohletz* [1989*a*]. The solutions are obtained by a simplified (explicit) variation of the implicit multifield finite difference solution technique [*Harlow and Amsden*, 1975; *Wohletz et al.*, 1984; *Valentine and Wohletz*, 1989*a*; *Wohletz and Valentine*, 1990].

The numerical implementation of the equations assumes cylindrical symmetry of the plumes or flows and of objects in the ground boundary layer [*Valentine et al.*, 1991]. The computational domain consists of a 7 km × 7 km box that is evenly divided into finite difference cells with dimensions of 100 m × 100 m (Figure 1). The box represents a half-space of a cylindrical system, with the left-hand boundary being the symmetry axis. The upper and right-hand boundaries are defined as zero gradient boundaries so that they allow outflow or inflow as determined by the interior calculation. The bottom boundary is a free-slip, reflecting boundary. Cells on the left end of the bottom boundary represent the volcanic vent (also referred to as the exit plane); gas and ash flux, along with temperature and pressure, are defined at these cells. A simple annular obstacle can be represented by adding a block into the bottom boundary. The boundary conditions and resolution are chosen to model the large-scale

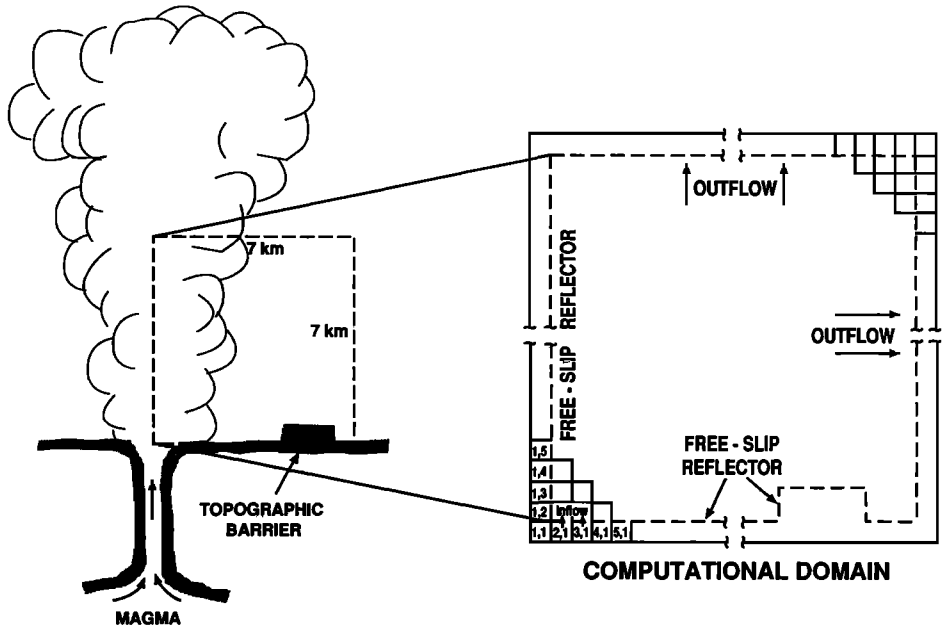

Fig. 1. The finite difference computational domain. For future reference, the two numerical simulations discussed in this paper are simulation 107 (has a caldera rim simulated on the bottom boundary), and simulation 121 (flat bottom boundary). Boundary conditions are discussed in the text.

dynamics of pyroclastic fountains and as such do not resolve many of the more detailed boundary layer processes that are preserved in volcanic deposits (for example, interaction with small-scale topography and erosion or deposition on the meter or 10-m scale).

Description of the Numerical Simulations

The exit plane conditions for the simulations are as follows: exit velocity (ash and gas) is 300 m/s, volatile (H_2O) mass fraction is 0.74%, exit pressure is 0.1 MPa, vent radius is 200 m, temperature (gas and ash) is 1200 K, ash particle diameter is 2.0 cm, and material density of the particles is 2400 kg/m^3. The mass flux of solids at the vent is 9.8×10^8 kg/s, which is believed typical of an intermediate-volume silicic eruption. The atmosphere is initially isothermal (300 K) and density stratified.

Numerical analyses have shown that topography around the vent can have a strong influence on column and pyroclastic flow properties [*Valentine et al.*, 1991]. We therefore examined two cases for this work: (1) an eruption from a vent surrounded by flat terrain; and (2) an eruption from a central vent surrounded by a simulated caldera rim. We approximate the topographic rim by an annulus that is rectangular in cross section (Figure 1). The topographic rim was chosen to be typical in location and size for an intermediate-volume caldera, although these values vary widely from one volcano to another. For the case examined here, the inner edge of the caldera rim is 4.0 km from the vent and is 500 m high by 1.5 km wide.

Consecutive snapshots of the simulation for the case with a caldera rim are shown in Plate 1. Snapshots for the simulation without an obstacle are in a general way similar to those shown in Plate 1 except that pyroclastic flows move continuously outward and are not confined by the caldera rim (see bottom frames in Plate 1). At a more detailed scale of both time and space, the rim influences the eruptive phenomena, as discussed below and by *Valentine et al.* [1991].

Initially the eruption produces a jet penetrating into the atmosphere. The top of the jet (termed the working surface or starting vortex [*Norman et al.*, 1982; *Kieffer and Sturtevant*, 1984]) is characterized by a wide, ring-vortex structure. In the case studied, the jet rises to an altitude of about 4.5 km, by which its initial kinetic energy and some of its thermal energy is converted into potential energy.

The gas and ash mixture is denser than the atmosphere, so it falls back toward the ground in a process that is commonly termed column collapse [*Smith*, 1960; *Sparks et al.*, 1978]. From the time the collapsing column impacts the ground, the eruption is said to have a fountain structure [*Valentine and Wohletz*, 1989*a*]. Most of the erupted material flows radially outward as a pyroclastic flow, but some is recirculated inwardly, reentering the column. The acceleration of this recirculated material upward into the jet extracts some of the momentum from the base of the column, causing a decrease in fountain height.

A low-concentration cloud rises buoyantly above the fountain and pyroclastic flows. The cloud is mushroom-shaped with a flared base that extends to cover the pyroclastic flows. In the middle it is narrower but variable in width, and at the top the working surface has a large diameter. Ash rises above the fountain and the laterally moving flows because of mixing (more properly termed turbulent diffusion in our model) of clean atmosphere into some of the gas/ash mixture. This process heats admixed gas, and if the local particle concentration is low enough, the new mixture can be positively buoyant. The column produced over the fountain is called a co-ignimbrite cloud, and some aspects of its dynamics have been discussed by *Valentine and Wohletz* [1989*a*] and *Woods and Wohletz* [1991]. The fallout deposits from these clouds can be of considerable volume (hundreds of cubic kilometers) and quite widely dispersed [*Rose and*

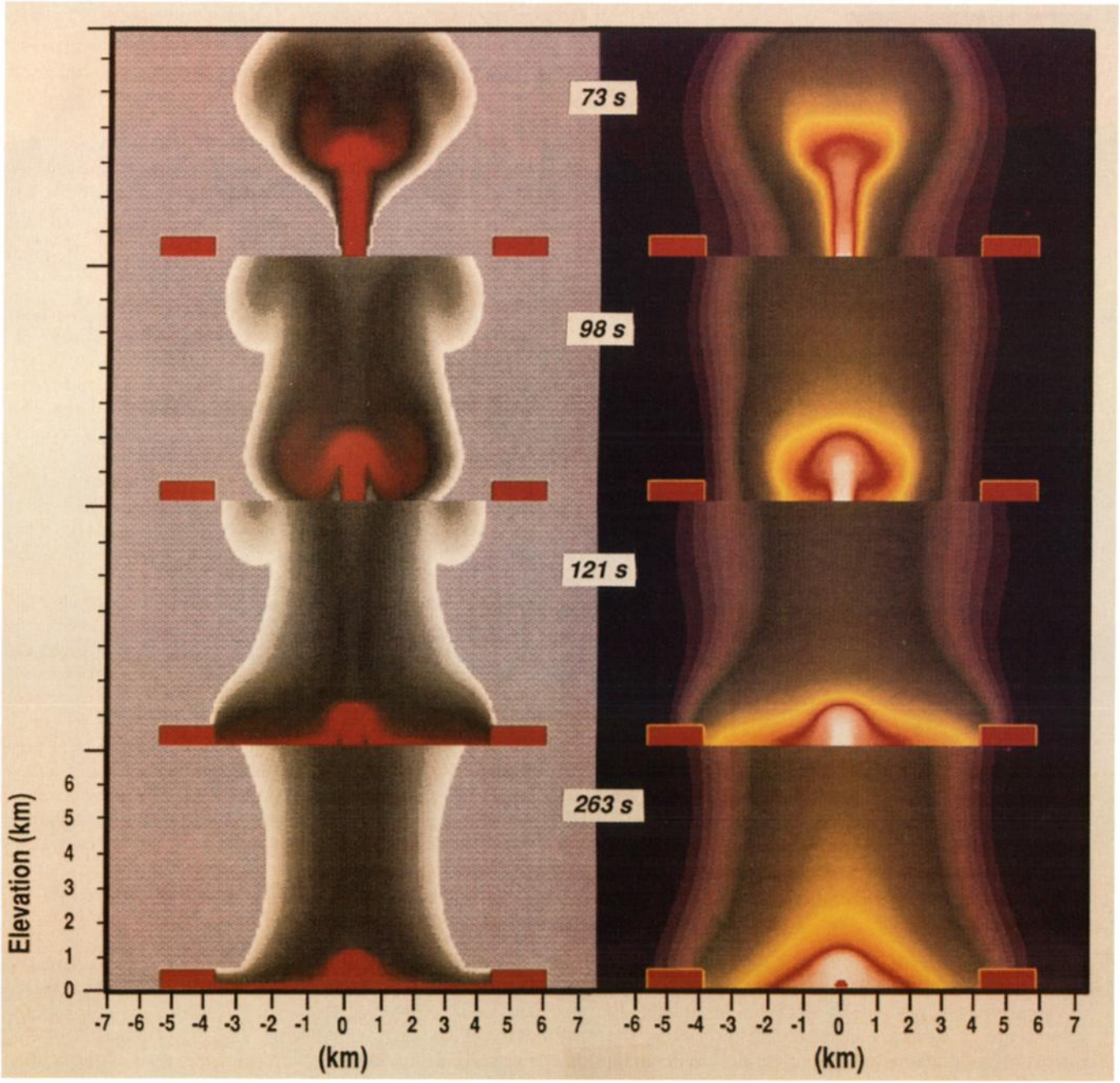

Plate 1. Snapshots at t = 73 (top), 98, 121, and (bottom) 263 s after eruption initiation. Vertical scale on each snapshot is 7 km; horizontal scale is 14 km with the vent located in the center (7 km). The rectangular blocks at each side of the eruption represent a caldera rim. Note that calculations are carried out in a half-space, the output is then reflected produce a mirror image for visualization purposes. (Left) Ash volume fraction, decreasing from maximum values of $\sim 10^{-3}$ (red) to 10^{-8} (white). Light blue background is clean atmosphere. (Right) Gas temperature with a maximum of 1200 K (white), decreasing through red to yellow to blue. Initial ambient temperature is 300 K.

Chesner, 1987]. To the extent that the distribution of fallout deposits is caused by the vent and column dynamics (in contrast, say, to the additional effects of atmospheric winds), the time-variable behavior discussed here will be reflected in fallout deposits (e.g., the position of isopleths).

An eruption-induced atmospheric wind, which is drawn inward toward the vent and upward with the co-ignimbrite plume, develops as the eruption progresses. This wind exerts a drag force on the top of the pyroclastic flow and thus draws material from the pyroclastic flow back toward the eruption column and into the co-ignimbrite plume.

The pyroclastic flow continues to move outward until it encounters the topographic barrier at 4 km distance (if there is no barrier, the pyroclastic flow simply continues flowing outward beyond 4 km). At this distance the pyroclastic current has a lateral velocity of c. 50 m/s. The current "swashes" up the stoss side of the obstacle, but in the simulation examined here, the pyroclastic flow does not have enough momentum to flow over it. Video animations of the calculation show that the "swash" forms a gravity wave that propagates back toward the vent. The structure of the gravity wave is complex because the fluid through which it

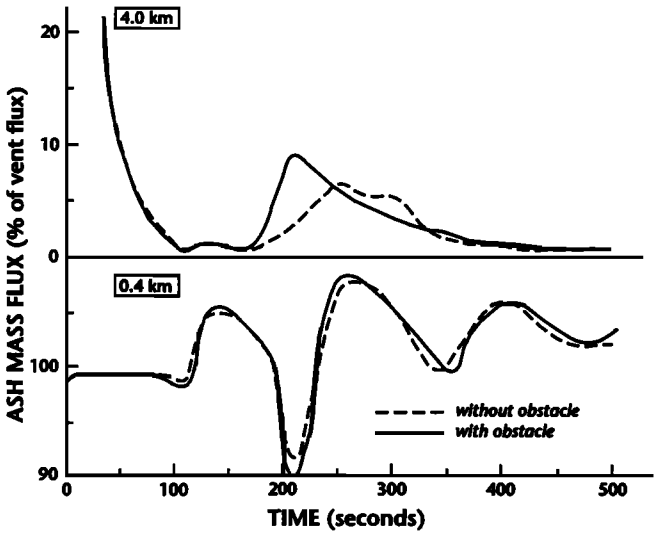

Fig. 2. Plots of solids mass flux at 0.4 and 4.0 km elevation as functions of time. Values are given in terms of percentage of vent mass flux.

propagates does not have a density interface as would be described by classical hydraulic analysis. Instead, the fluid (referring to the gas/ash mixture) has a continuously decreasing density with height because of turbulent diffusion. At any given location the gravity wave speed varies with height, and is not a single constant value because of this density structure [*Valentine*, 1987].

The eruption-induced atmospheric wind exerts a ventward drag force on the top of the propagating gravity wave. For a short time the wind-wave interaction causes the wave to take on the form of an ocean wave breaking as it approaches a shore. As the wave moves closer to the vent, it begins to lose its form, and the upper part of it is drawn upward and inward into the co-ignimbrite plume where it becomes a hot "bulge" that rises in the plume.

INTERPRETATION OF SOURCES OF UNSTEADINESS

Three proposed sources of mass flux unsteadiness in the column are (1) increase in mass flux just above the vent caused by recirculation of pyroclastic flow material into the base of the column; (2) buoyant ash that rises from the pyroclastic flow and is swept back into the column at higher levels by the ventward wind; and (3) internal waves moving in the pyroclastic flow back to the vent after the flow has impinged upon a topographic obstacle. Figure 2 is a plot of ash mass flux versus time at two levels above the vent for the simulations described above. The plots at 0.4 km correspond to the basal gas thrust region of the fountain. The 4.0-km elevation plots correspond to the co-ignimbrite plume above the fountain. The mass flux is plotted as a percentage of the vent flux.

The mass fluxes of ash at 0.4 km and 4.0 km show two or more peaks (Figure 2). As the eruption begins, the mass flux at 0.4 km above the vent increases from zero (the preeruptive state) to that at the vent by $t \sim 5.0$ s. The working surface passes through 4.0 km at $t \sim 25$ s, producing a mass flux peak of about 50% that at the exit plane; it then falls rapidly off to values of several percent.

After column collapse begins (at $t \sim 110$ s) there is a sharp rise in mass flux at 0.4 km, and by $t = 140$ s the flux reaches values about 5% greater than that at the vent. This increase is caused by the reincorporation of ash that has collapsed back through the fountain (described in more detail by *Valentine and Wohletz* [1989*a*, *b*] and *Valentine et al.* [1991]). This reincorporation or recirculation phenomenon perturbs the column mass flux and drives an oscillatory unsteadiness that damps with time; these oscillations are ±10% of the vent value, with a period of about 130 s. As these oscillations damp with time, the mass flux at an elevation of 0.4 km approaches steady values of about 5% greater than that of the vent.

At 4.0-km elevation the second peak in mass flux, equal to about 10% of that at the vent, occurs at $t = 210$ s (Figure 2). This peak can be attributed partly to propagation of the initial mass flux peak that is observed at 0.4 km and is the final oscillation observed within the coignimbrite plume. The driving mechanism of this oscillation at 4 km reflects contributions from all three sources of unsteadiness listed above. Because the later oscillations that occur in the interior of the fountain structure (as recorded at 0.4-km elevation) are not observed in the co-ignimbrite plume, it appears that the main source of ash in the plume is the reentrainment of ash off the top of the pyroclastic flow.

For low-level (0.4 km) mass flux unsteadiness, the effect of the topographic obstacle is very small (Figure 2). This result apparently reflects the fact that the recirculation of pyroclastic backflow, which dominates the fluctuations at this level, all occurs well within the radius of the topographic rim in this simulated eruption. However, at 4.0 km the mass flux peak in the obstacle case is about 40 s earlier and is relatively stronger than the peak in the no-obstacle case. This difference can be attributed to the influence of the gravity waves on the entrainment of ash swept off the top of the pyroclastic flows (the source most of the ash in the co-ignimbrite plume, as described above).

To examine temporal temperature variations in detail, ash and gas temperature versus radius within the column, at 4.0-km elevation, were plotted at $t = 110$, 160, and 230 s (Figure 3). For all times, the gas temperature decreases outward toward the column edge, tending toward the ambient value of 300 K. The solid fragments are consistently hotter than the gas, reflecting the thermal inertia of the relatively large particles (2-cm diameter) used in this model. For the first several minutes of the eruption, the hotter solids reside toward the edge of the column, and this temperature distribution only reverses at later times ($t \sim 4$ min) when relatively steady conditions have been established in the column.

INFLUENCES ON REMOTE OBSERVATION

Remote observations of eruptions commonly record parameters related to cloud temperature (e.g., infrared intensity), ash concentration (opacity), and plume diameter. Variations in temperatures and ash concentrations at the plume centerline, at an elevation of 7 km, are qualitatively similar for flows with and without the caldera rim (Figures 4*a*–4*c*). Temperatures show an early maximum at $t \sim 110$ s for the gas and $t \sim 60$ s for the ash, followed by a decrease to about 450 K for both gas and ash at $t \sim 180$ s, and then a second maximum at 230–250 s.

The initial temperature maximum is caused by the passage

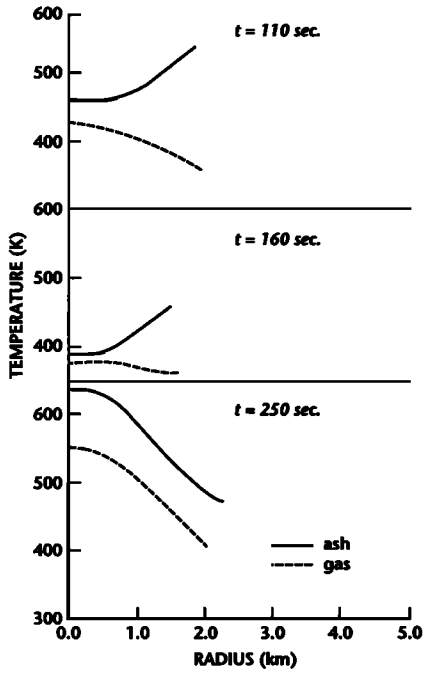

Fig. 3. Temperature versus radius in the co-ignimbrite plume at 4 km altitude for times t = 110 s (top), 160 s, and 250 s (220 s for the simulation with the flat boundary).

of the working surface through the 7-km elevation. As the jet collapses into the fountain stucture, rising ash experiences more mixing with the cool atmosphere so that the centerline temperature decays to the minimum at t = 180 s. After the fountain collapse occurs, a second source of hot material is available to the eruption column, namely, ash from the developing pyroclastic flows that is drawn back toward the column.

In the case where a caldera rim is present, the reflecting gravity wave forms at $t \sim 120$ s and travels back toward the vent, where it is eventually drawn upward into the co-ignimbrite plume. The material in the wave is hot ash and gas derived directly from the pyroclastic flow, resulting in the second temperature maximum at $t \sim 230$ s. The ash volume fraction increases continuously until $t \sim 200$ s, after which it decreases slightly until t = 230 s. Interestingly, the brief decrease in ash concentration occurs at the same time as the second temperatrue maximum and may be caused by gas expansion at the higher temperature. The drawn-up wave does cause a brief increase in the total mass flux of ash in the buoyant plume (Figure 2), but is manifested as a temporary increase in the plume radius instead of as a peak in the ash concentration at a specific point.

The plume radius at 7-km elevation shows two maxima both for eruption with and without an obstacle (Figure 4*d*).

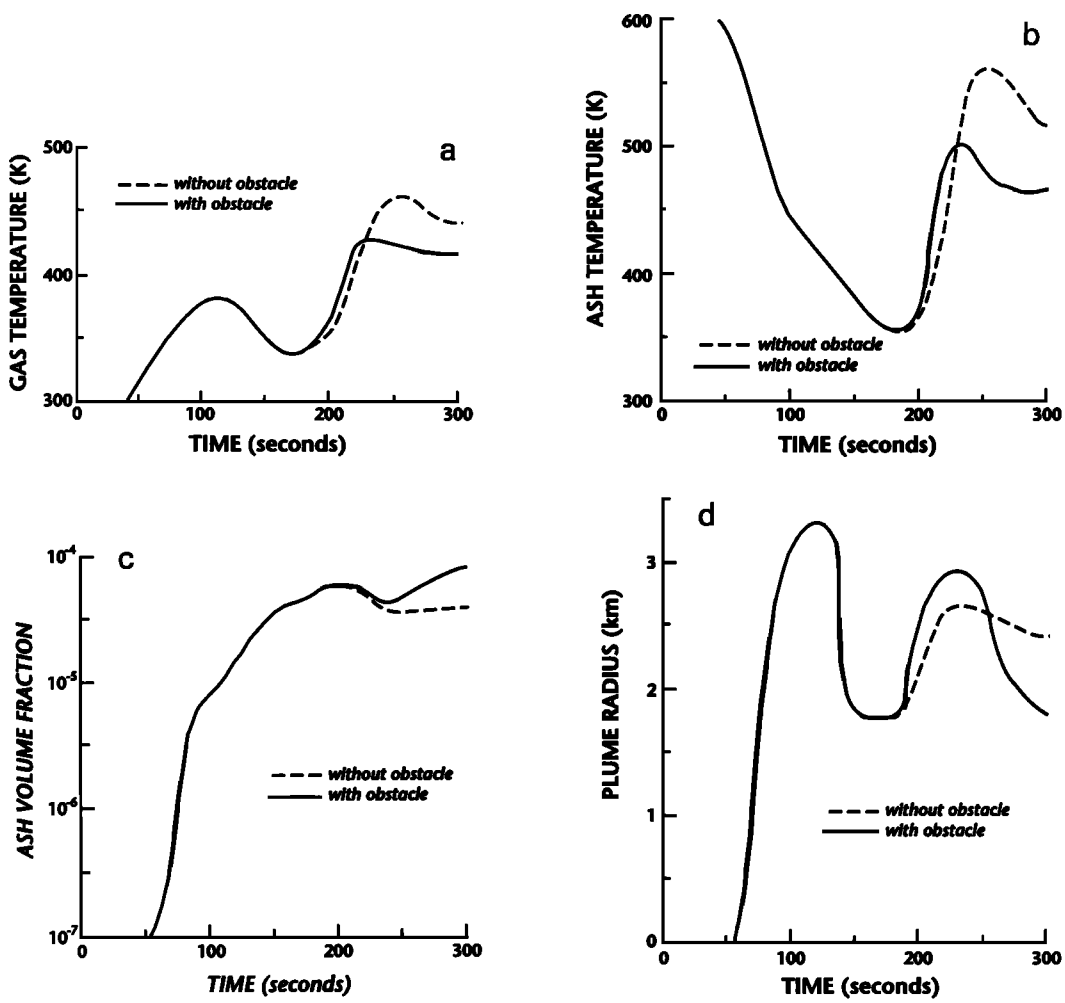

Fig. 4. Centerline values of (*a*) gas temperature, (*b*) ash temperature, and (*c*) ash volume fraction at 7-km elevation, as functions of time, (*d*). Also shown is plume radius as a function of time at 7-km elevation.

The first maximum occurs at t = 110 to 120 s and corresponds to the passage of the working surface. The second maximum occurs approximately at t = 230 s and corresponds to the initial pulse of ash that is drawn off the top of the pyroclastic flows. This second maximum is stronger in the simulation with a topographic obstacle. Again, this effect is attributed to the influence of the gravity wave that is reflected when the pyroclastic flows encounter the obstacle. The final "steady" radius is about 2.4 km for the eruption with no obstacle and 1.7 km for the eruption with an obstacle. This results from the larger areal extent of the pyroclastic flows which feed the co-ignimbrite plume when they are not impeded by topography.

CONCLUSIONS AND INFERENCES

For a remote observer measuring plume diameter or for a satellite recording infrared emissions from the plume top, the complicated mass flux and temperature structures may be misleading. In particular, the second thermal pulse and increase in plume diameter (Figure 4) may be interpreted as a second explosive event (i.e., an increase in mass flux at the vent), when in reality these events are inherent in the fluid dynamical processes occurring during unsteady flow at the onset of the eruption. This problem would be confounded by the fact that the events beneath the co-ignimbrite cloud, but within the fountain structure, are likely to be obscured by ash. Variations in plume diameter during the unsteady flow will influence ejecta dispersal patterns preserved in the coignimbrite deposits. In particular, variation of the isopleth positions would be likely. Although our calculation imposes a cylindrical symmetry, we speculate that any large obstacle with a height that is of the same order as the pyroclastic flow thickness could contribute to variations in the column properties by generation of reflected waves.

Finally, we comment on the single published example of a double temperature pulse that has been documented in the literature: that observed by satellite during the May 18, 1980, eruption at Mount St. Helens [*Moore and Rice*, 1984; *Sparks et al.*, 1986]. A second thermal pulse in the eruption cloud was recorded at approximately the same time (1500:34.5 hours) that the pyroclastic current encountered its first major topographic obstacle (the north wall of the Toutle River Valley and high country continuing to the north). The results of the numerical simulation presented here cannot be applied directly to Mount St. Helens because of the asymmetry of the lateral blast, but we believe that at least two of the processes that we have discussed could have contributed to the double temperature pulse observed: entrainment of material from the pyroclastic flow (also called the blast surge [*Fisher*, 1990] into the rising column, and addition of material from a gravity wave reflected from the north wall of the Toutle River Valley.

Numerical studies such as the one discussed here, combined with advanced visualization technology, can provide much insight into natural processes and can help guide observations and interpretations. While difficult to apply to specific locales and observations because of the complexity of the real world, knowledge of processes gained from the simulations can lead to constraints on observations that have multiple interpretations and can help in guiding formulation of testable models from field observations. We hope that large-scale computation will gain an increasingly important role in the observational earth sciences.

Acknowledgments. This work is supported by the U.S. Department of Energy's Laboratory Directed Research and Development funds at Los Alamos National Laboratory. Grant Heiken and Richard Warren provided helpful reviews of the manuscript. The work of S. W. Hodson and L. MacDonald with visualization of simulation results has been essential in improving our understanding of the simulation dynamics. We thank Mary Ann Olson for drafting the illustrations.

REFERENCES

Carey, S., and R. S. J. Sparks, Quantitative models of the fallout and dispersal of tephra from volcanic eruption columns, *Bull. Volcanol.*, *48*, 109–126, 1986.

Fisher, R. V., Transport and deposition of a pyroclastic surge across an area of high relief: The 18 May 1980 eruption of Mount St. Helens, Washington, *Geol. Soc. Am. Bull.*, *102*, 1038–1054, 1990.

Harlow, F. H., and A. A. Amsden, Numerical calculation of multiphase fluid flow, *J. Comput. Phys.*, *17*, 19–52, 1975.

Kieffer, S. W., and B. Sturtevant, Laboratory studies of volcanic jets, *J. Geophys. Res.*, *89*, 8253–8268, 1984.

Moore, J. G., and C. J. Rice, Chronology and character of the May 18, 1980, explosive eruptions of Mount St. Helens, in *Explosive Volcanism: Inception, Evolution, and Hazards*, pp. 133–142, National Academy Press, Washington, D. C., 1984.

Norman, M. L., L. Smarr, K. H. A. Winkler, and M. D. Smith, Structure and dynamics of supersonic jets, *Astron. Astrophys.*, *113*, 285–302, 1982.

Rose, W. I., and C. A. Chesner, Dispersal of ash in the great Toba eruption, 75 ka, *Geology*, *15*, 913–916, 1987.

Smith, R. L., Ash flows, *Geol. Soc. Am. Bull.*, *71*, 795–842, 1960.

Sparks, R. S. J., L. Wilson, and G. Hulme, Theoretical modeling of the generation, movement, and emplacement of pyroclastic flows by column collapse, *J. Geophys. Res.*, *83*, 1727–1739, 1978.

Sparks, R. S. J., J. G. Moore, and C. J. Rice, The initial giant umbrella cloud of the May 18th, 1980, explosive eruption of Mount St. Helens, *J. Volcanol. Geotherm. Res.*, *28*, 257–274, 1986.

Valentine, G. A., Stratified flow in pyroclastic surges, *Bull. Volcanol.*, *49*, 616–630, 1987.

Valentine, G. A., and K. H. Wohletz, Numerical modeling of Plinian eruption columns and pyroclastic flows, *J. Geophys. Res.*, *94*, 1867–1887, 1989*a*.

Valentine, G. A., and K. H. Wohletz, Environmental hazards of pyroclastic flows determined by numerical models, *Geology*, *17*, 641–644, 1989*b*.

Valentine, G. A., K. H. Wohletz, and S. W. Kieffer, Effects of topography on facies and compositional zonation in caldera-related ignimbrites, *Geol. Soc. Am. Bull.*, in press, 1991.

Wohletz, K. H., and G. A. Valentine, Computer simulations of explosive volcanic eruptions, in *Magma Transport and Storage*, edited by M. P. Ryan, pp. 114–135, John Wiley, New York, 1990.

Wohletz, K. H., T. R. McGetchin, M. T. Sandford II, and E. M. Jones, Hydrodynamic aspects of caldera-forming eruptions: Numerical models, *J. Geophys. Res.*, *89*, 8269–8286, 1984.

Woods, A. W., The fluid dynamics and thermodynamics of eruption columns, *Bull. Volcanol.*, *50*, 169–193, 1988.

Woods, A. W., and K. H. Wohletz, Dimensions and dynamics of co-ignimbrite eruption columns. *Nature*, *350*, 225–227, 1991.

S. W. Kieffer, Department of Geology, Arizona State University, Tempe, AZ 85287.

G. A. Valentine, Mail Stop F665, Geoanalysis Group, Earth and Environmental Sciences Division, Los Alamos National Laboratory, Los Alamos, NM 87545.

K. H. Wohletz, Mail Stop D462, Geology-Geochemistry Group, Earth and Environmental Sciences Division, Los Alamos National Laboratory, Los Alamos, NM 87545.

(Received May 6, 1991;
accepted August 9, 1991.)